Design and Performance of Field Regulated Reluctance Machine

Joseph D. Law, *Member, IEEE,* Allen Chertok, *Member, IEEE,* and Thomas A. Lipo, *Fellow, IEEE*

Abstract—A unique topological configuration for rotating electromagnetic machines that can produce significantly higher force density than an induction machine is investigated. The stator is constructed using full pitch concentrated windings embedded in conventional slots. Rotor saliency is produced using poles constructed of axially oriented laminations. Operation is such that all of the conductors are actively taking part in torque production all of the time. The means for exciting the stator windings allows for independent control of torque and regulation of the rotor flux. A force density comparison is made based on operation with equal surface current density, conduction losses, and peak air-gap flux density. Construction and testing of a prototype 500-rpm, 28-kW laboratory machine, converter, and controller are described.

I. INTRODUCTION

IN spite of continuous progress in the design of variable speed ac motor drives throughout the last three decades, except for minor modifications to accommodate the increased heating due to harmonics, relatively little attention has been paid to improvement in the design of the ac motor used for such applications. In this paper the inherent performance characteristics of a new type of ac machine termed a field regulated reluctance machine (FRRM) are established. Models are developed for prediction of the steady-state performance. The force density advantage of an FRRM over an induction machine of equivalent size is investigated. An example design and the performance characteristics of a 100-kW generator with an air-gap force density of 40 kN/m² are presented. The models are verified by means of laboratory tests of a 28-kW FRRM, converter, and controller.

II. LITERATURE REVIEW

The principles of operation of a new type of machine, defined in this paper as a field regulated reluctance machine, have been introduced relatively recently by Weh [1]. The motivation of this work was to design a machine

inherently capable of high power density. Reluctance machines, with their passive rotor structures, typically permit high rotational speeds. In addition, by optimizing the winding configuration, phase currents, and rotor configuration, machines with high power densities can be obtained.

The concept of interleaving layers of material with low magnetic permeance between the iron laminations on the rotor to control armature reaction of the FRRM has been presented by Weh and Schröder [2]. Reference [3] presents an FRRM used in an application for which it is well suited: a flywheel energy storage system. Active compensation of armature reaction using ferrite permanent magnets suitably placed in the rotor has been investigated by Mayer, Mosebach, Schröder, and Weh [4]. The selection of pole pitch is presented in detail and selection of the slot opening is somewhat dealt with by Boldea and Nasar [5].

However, none of these papers discuss the performance details of this machine, particularly the important limiting effects of saturation. This paper presents a detailed investigation into the principle of operation of this new machine and its behavioral characteristics as a result of saturation, as well as the development of suitable mathematical tools for the design of such machines. In addition, an example design including selection of design parameters such as the phase number, pole arc, slot opening/tooth pitch, etc. is presented.

III. PRINCIPLES OF OPERATION

A cross-sectional view, Fig. 1, shows the basic elements of a typical FRRM. In such a machine, rotor saliency is produced using poles constructed of axially oriented laminations [6].

In general, an FRRM is constructed using full pitched concentrated windings embedded in a conventional slotted stator. In this case operation is such that all of the conductors are actively taking part in torque production all of the time, whereas in conventional three-phase square-wave current source excitation, only two of the three phases are actively producing torque.

Individual windings are operated in a time share mode; for a portion of time each stator winding acts as the excitation (field) winding and for a portion of time as the armature winding. The mode of operation for a particular winding is dependent on the rotor position. During the period when the coils of a particular winding are located
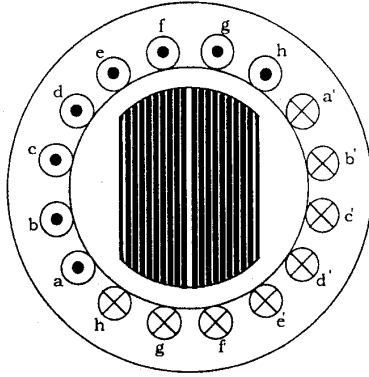
Fig. 1. Simplified cross-sectional view of a field regulated reluctance machine.

Fig. 2. Idealized current and voltage waveforms of one phase of a field regulated reluctance motor.

under the pole faces, the current flowing in them corresponds to and is controlled as the equivalent of an armature current of a dc motor. While the coils of a winding are located in the interpole space, the current flowing in them corresponds to and is controlled as field current. This mode of exciting the stator windings allows for independent control of torque and regulation of the field (i.e., magnetizing) flux. Fig. 2 shows the resulting idealized winding current and voltage waveforms versus time for motor operation. Note that the counter emf due to rotor rotation occurs only when the flux is changing.

IV. FORCE DENSITY CONSIDERATIONS

A. Force Density

Force density for rotating electric machinery is typically defined as the tangential force (force of rotation) per unit area of the air-gap. For design purposes it is useful to consider a lossless m-phase FRRM having C parallel circuits per phase. Assuming idealized FRRM current and voltage waveforms versus time, Fig. 2, the output power of the machine is given by

$$P_{\text{out}} = m_q V_s L_{\text{arm}}, \tag{1}$$

where m_q is the number of q-axis phases, V_s is the rated peak voltage, and I_{arm} is the rated peak armature current per phase.

Assuming constant mechanical radian frequency and ignoring the spatial flux variation under a pole, Fig. 3 shows the flux linking one full pitch turn versus electrical angle. By inspection of Fig. 3, the magnitude of the derivative of flux linking one turn with respect to electrical angle, θ_{elect}, can be rewritten for the portion of time it is nonzero as

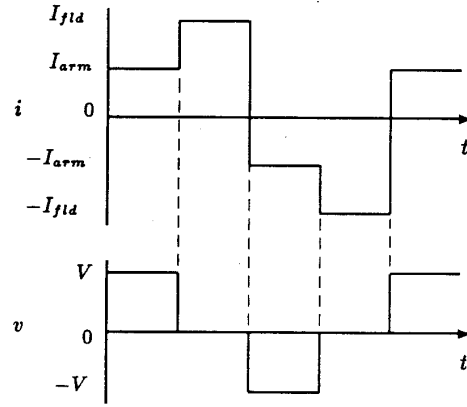$$\frac{d\phi_p}{d\theta_{\text{elect}}} = 2\phi_{\max}\left(\frac{m}{m_q\pi}\right), \tag{2}$$

or, in terms of time,

$$\frac{d\phi_p}{dt} = 2\phi_{\max}\left(\frac{m}{m_q\pi}\right)\left(\frac{\mathscr{P}\omega_m}{2}\right), \tag{3}$$

where $\phi_{\max}$ is the peak flux linking one turn, m is the total number of phases, θ_m is the mechanical angle, $\mathscr{P}$ is the number of poles, and ω_m is the mechanical radian frequency.

The peak flux linking one turn is related to the air-gap flux density by

$$\phi_{\max} = B_{\text{avg}} R_{is} l_e\left(\frac{m_q}{m}\right)\left(\frac{2\pi}{\mathscr{P}}\right), \tag{4}$$

where B_{avg} is the average flux density, R_{is} is the inner stator radius, and l_e is the effective stack length. If stator leakage inductance and resistance are neglected, then by substituting (4) into (3) and multiplying by N_t, the number of turns/(phase · circuit), yields

$$V_s = 2N_t B_{\text{avg}} R_{is} l_e \omega_m. \tag{5}$$

The surface current density can be quantified by forming an expression for the rms current per unit length of the air-gap circumference. The rms current per circuit is related to the rated peak armature by

$$I_{\text{rms}} = \left(\frac{m_q + m_d R_{f/a}^2}{m}\right)^{1/2}\left(\frac{I_{\text{arm}}}{C}\right), \tag{6}$$

where m_d is the number of field phases and $R_{f/a}$ is the ratio of peak field current to peak armature current. The ratio $R_{f/a}$ is fixed for a given machine operating at rated speed, torque, and voltage.

Neglecting time shifts, the current waveforms are identical in each of the phases. Therefore, the rms current is the same in each coil. Furthermore, every coil is full pitched. Under these conditions,

$$A_s = \left(\frac{2mCN_t}{2\pi R_{is}}\right)\left(\frac{m_q + m_d R_{f/a}^2}{m}\right)^{1/2}\left(\frac{I_{\text{arm}}}{C}\right), \tag{7}$$
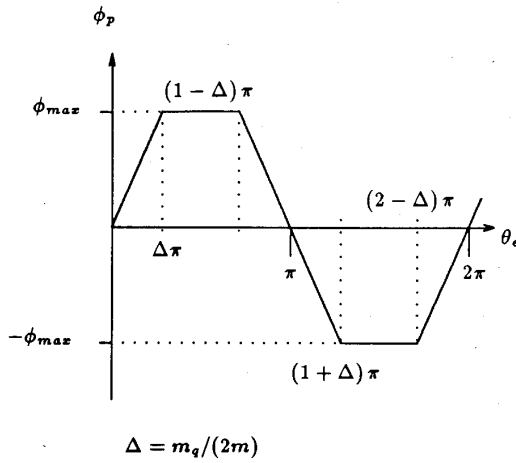
$$\Delta = m_q/(2m)$$

Fig. 3. Flux linking one turn versus electrical angle.

where A_s is the rms current per unit length of the air-gap circumference.

Solving (7) for the peak per-phase armature current gives

$$I_{\mathrm{arm}} = \left(\frac{2\pi R_{is}}{2mN_t} \right) \left(\frac{m}{m_q + m_d R_{f/a}^2} \right)^{1/2} A_s. \qquad (8)$$

Substituting (5) and (8) into (1) yields

$$P_{\mathrm{out}} = \left(\frac{m_q}{m} \right) \left(\frac{m}{m_q + m_d R_{f/a}^2} \right)^{1/2} B_{\mathrm{avg}} A_s (2\pi R_{is}^2 l_e) \omega_m. \qquad (9)$$

It is convenient to define a *current utilization factor*

$$k_I \equiv \left(\frac{m_q}{m} \right) \left(\frac{m}{m_q + m_d R_{f/a}^2} \right)^{1/2}. \qquad (10)$$

Making use of k_I, (9) can be written as

$$P_{\mathrm{out}} = k_I B_{\mathrm{avg}} A_s (2\pi R_{is}^2 l_e) \omega_m. \qquad (11)$$

Eq. (11) expresses the output power of an FRRM in terms of conventional sizing equation parameters and an additional factor, the current utilization factor. The current utilization factor k_I is a measure of the utilization of the surface current density as armature current. Furthermore, the maximum value of the utilization is always less than 1. As such, it is similar to the power factor of an induction machine.

The force per unit air-gap area is obtained by normalizing by the appropriate terms, whereby

$$f_{\mathrm{area}} = k_I B_{\mathrm{avg}} A_s. \qquad (12)$$

B. Utilization Factors

1) Current Utilization Factors: Three factors can be identified that are measures of the utilization of the surface current. The current utilization factor (defined in (10)) is a measure of the utilization of the surface current density as armature current. To assist in understanding the current utilization factor, it is expressed as the product of two factors:

$$k_{I1} = \left(\frac{m_q}{m} \right), \qquad (13)$$

$$k_{I2} = \left(\frac{m}{m_q + m_d R_{f/a}^2} \right)^{1/2}. \qquad (14)$$

The first term, k_{I1}, is the fraction of the air-gap circumference available to be used for armature current. The second term, k_{I2}, is a measure of how well the number of phases are divided between field and armature phases. For a sufficiently large number of phases, the distribution between field and armature phases can be thought of as the division of a continuum.

Ignoring armature reaction and the temporal flux variation, a maximum force density is achieved with designs in which the peak field current equals the peak armature current and m_d equals the required fraction that produces the desired air-gap flux density. For designs that satisfy the above condition, k_{I2} has a value of 1. Values of k_{I2} greater than 1 indicate that the armature current is greater than the field current, a suboptimal design. Values of k_{I2} less than 1 indicate that the armature current is less than the field current, also a suboptimal design.

To further investigate the current utilization factor, it is assumed that an "optimal" machine has been designed with a division of m between m_q and m_d such that k_I is a maximum and a desired B_{ave} is obtained. Fig. 4 shows the factors k_{I1}, k_{I2}, and k_I versus m_d for an FRRM in which $C = 1$, $m_d I_{fld} = 4.0$ $m = 9$, and $I_{\mathrm{rms}} = 1.33$. For values of m_d less than 1.00, the desired product of m_d with the field current cannot be obtained while also maintaining I_{rms} at 1.33.

2) Flux Utilization Factors: The flux utilization factors relate the average air-gap flux density to the peak air-gap flux density. Making use of the flux utilization factors, the expression for f_{area}, (12), can be rewritten in terms of the peak air-gap flux density. Average air-gap flux density B_{avg} is related to the peak air-gap flux density B_{pk} by

$$B_{\mathrm{avg}} = k_{ar} k_{fv} B_{\mathrm{pk}}. \qquad (15)$$

The utilization factor k_{ar} accounts for armature reaction and k_{fv} accounts for flux variation as the rotor of the FRRM turns through one phase pitch. A phase pitch is defined as the product of the number of adjacent slots per pole with coils of the same phase and the slot pitch. Variation of flux as the rotor turns through one phase pitch is due to the change in effective field mmf and the stator slots. The flux utilization factors are developed independent of each other.

Ignoring slot effects and constraining the radian angular frequency and the armature current to zero, the air-gap
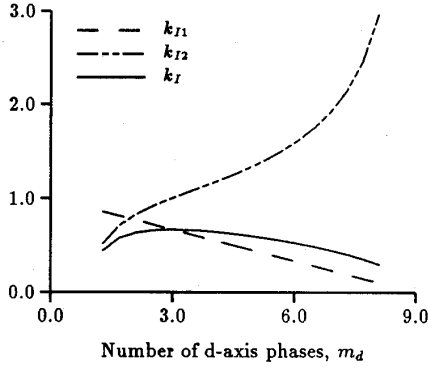
Fig. 4. The factors k_{I1}, k_{I2}, and k_I for an FRRM in which $C = 1$, $m_d I_{fld} = 4.0$, $m = 9$, and $I_{rms} = 1.33$.

flux density is uniform under a pole face. Under these conditions, the average air-gap flux density is given by

$$B'_{avg} = \left(\frac{m}{m_q}\right)\left(\frac{\mathscr{P}}{2\pi R_{is}l_e}\right)\left(\frac{\mathscr{P}}{N_t C^2}\right)m_d L_d I_{fld}, \quad (16)$$

where L_d is the d-axis air-gap inductance per coil. Assuming linear iron and a nonzero value for I_{arm}, the average air-gap flux density is still given by (16), but the peak air-gap flux density under a pole face is

$$B'_{pk} = \left(\frac{m}{m_q}\right)\left(\frac{\mathscr{P}}{2\pi R_{is}l_e}\right)\left(\frac{\mathscr{P}}{N_t C^2}\right)$$
$$\cdot \left(m_d L_d I_{fld} + \frac{1}{2}m_q L_q I_{arm}\right), \quad (17)$$

where L_q is the q-axis air-gap inductance per coil. The ratio of B'_{avg} to B'_{pk} is

$$k_{ar} = \frac{2m_d L_d I_{fld}}{2m_d L_d I_{fld} + m_q L_q I_{arm}}. \quad (18)$$

Dividing (18) by I_{arm} and L_d,

$$k_{ar} = \frac{2m_d R_{f/a}}{2m_d R_{f/a} + m_q L_q / L_d}. \quad (19)$$

The need for k_{fv} is a result of a finite number of phases and a slotted stator. During rotation through one phase pitch, the function of one of the phases changes from an armature phase to that of a field phase. A semiempirical expression for the factor k_{fv} is

$$k_{fv} = \frac{4m_d R_{f/a} - 1}{4m_d R_{f/a}}. \quad (20)$$

Substituting the expression for B_{avg}, (15), into (12) results in an expression for force density in terms of peak flux density in the air-gap, rms surface current density, and utilization factors:

$$f_{area} = k_I k_{ar} k_{fv} B_{pk} A_s. \quad (21)$$

C. Comparison of the Force Densities of an FRRM and Induction Machine

The force density for a conventional induction machine is given by [8],

$$f_{area} = \frac{1}{\sqrt{2}}k_w B_{pk}\frac{A_{ti/m}}{(1 + \cos\phi)}\cos\phi, \quad (22)$$

where B_{pk} is the peak fundamental air-gap flux density, k_w is the winding factor, and $\cos\phi$ is the power factor. $A_{ti/m}$ is the total surface current density of an induction machine.

Eqs. (21) and (22) enable a comparison between the FRRM and the conventional squirrel cage induction machine based on equal peak air-gap flux density. Two comparisons are made assuming the following values of parameters for 1) an FRRM: $L_q/L_d = 0.200$, $R_{f/a} = 1.239$, $m = 7$, $m_q = 5$, $k_{ar} = 0.832$, $k_{fv} = 0.899$, $k_I = 0.6652$; and 2) an induction machine: $k_w = 0.900$ and $\cos\phi = 0.874$.

1) Comparison of Force Density given Equal Conduction Losses within the Bore: The ratio of FRRM force density, (21), to induction machine force density, (22), is given by (23), assuming equal a) weight of all conductors within the stack, b) total surface current densities, c) current densities, and d) peak flux densities:

$$R_{fd} = \sqrt{2}\left(\frac{k_{ar}k_{fv}k_I}{k_w}\right)\left(\frac{1 + \cos\phi}{\cos\phi}\right). \quad (23)$$

Using the values previously stated gives equal conduction losses within the stack, a ratio of force densities of 1.68, and a ratio of *stator* surface current densities of 1.874. That is, theoretically an FRRM can produce a 68% higher force density than an induction machine for the same conduction losses within the stack. The higher force density is made possible, in effect, by moving the unneeded rotor conducting material to the stator. However, space must clearly be found on the stator for a large slot cross-sectional area. Nonetheless, high force density electromagnetic designs for FRRM's clearly do exist with sufficiently large stator cross-sectional area.

The increase in stator slot leakage due to stator slots, as deep as those required in a high force density FRRM, would limit starting torque in an induction machine. However, simulations indicate that the relatively large slot leakage does not cause such problems with an FRRM. It has not been determined, however, whether locating all the losses on the stator will result in overheating of the windings.

2) Comparison of Losses given Equal Force Density: The ratio of FRRM to induction machine surface current density is given in (24), assuming equal a) force densities, b) weight of all conductors within the stack, and c) peak flux densities:

$$\left(\frac{A_s}{A_{ti/m}}\right) = \left(\frac{1}{\sqrt{2}}\right)\left(\frac{k_w}{k_{ar}k_{fv}k_I}\right)\left(\frac{\cos\phi}{1 + \cos\phi}\right). \quad (24)$$

Using the values previously stated gives a ratio of total surface current densities of 0.559. Therefore, the ratio of conduction losses within the stack of 0.3125, under the constraint of equal weight of conducting material. This comparison shows that for the same weight of conducting materials, an FRRM will generate significantly lower conduction losses than an induction machine if their force densities are the same.

V. DESIGN CONSIDERATIONS

The electromagnetic design of a machine requires making many choices, usually involving trade-offs with the mechanical design. A method for selection of essentially 23 major electromagnetic parameters is required for the design of an FRRM. The key specifications of a 100-rpm, 100-kW generator have been selected as the design example.

Since there are relatively few practical choices for the number of phases and the distribution of these phases between q-axis and d-axis phases, an exhaustive search has been used to determine the number of q-axis phases, the number of d-axis phases, and the q-axis and d-axis current magnitudes. Table I contains the resulting conduction losses as a function of the possible total number of phases and the distribution between d-axis and q-axis phases. The losses were calculated using a static magnetic circuit model [8]. A seven-phase machine with two phases serving as d-axis phases can be selected with the aid of Table I. It can be noted that while eight or nine phases generate lower losses, the slight decrease does not justify the increase in phase number.

Because losses are proportional to the square of the rms value of the current and not the average, the magnitudes of the d-axis and q-axis currents should be nearly the same. It appears that well-designed machines with reasonable air-gaps will require fewer d-axis (field component) phases than q-axis phases (armature component).

Fig. 5 shows the copper losses versus the number of poles for a seven-phase version of a 100-kW FRRM with a fixed air-gap radius. Conduction losses, in the portion of the conductors located within the stack of the machine, rise with an increase in the number of poles. The increase in losses within the stack of the machine is due to the increasing magnetizing requirement of the machine as the number of poles increases.

Table II contains the specifications and the predicted performance of the machine designed using the data of Table I and Fig. 5.

VI. EXPERIMENTAL MACHINE, CONVERTER, AND CONTROLLER

In order to validate the design procedure that has been developed, a small-scale, six-phase, 28-kW, 500-rpm machine was designed. To enable operation and testing of the experimental machine, a six-phase converter was also designed and constructed. Fig. 6 contains a block schematic of the converter and controller. A full bridge per phase is used to allow maximum control flexibility.
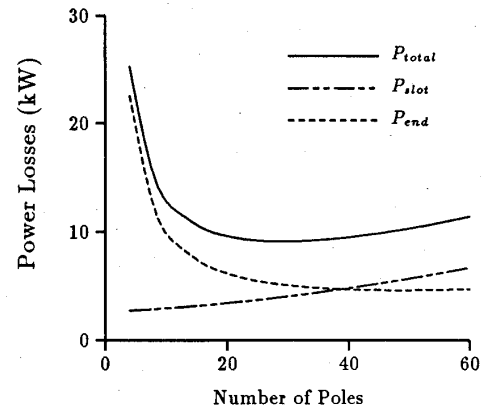

Fig. 5. Conduction losses versus number of poles for a seven-phase FRRM.

TABLE I
CONDUCTION LOSSES AS A FUNCTION OF NUMBER OF PHASES AND THE DISTRIBUTION OF PHASES BETWEEN d-AXIS AND q-AXIS PHASES FOR A 100-RPM, 100-kW FRRM.

Number of Phases	Power Losses (kW)	Number Field Phases/ Field Current	Number q-axis Phases/ q-axis Current
3	17.86	1/4.18	2/3.97
4	17.84	1/4.10	3/2.64
4	16.84	2/2.04	2/3.97
5	18.56	1/4.03	4/1.98
5	16.88	2/2.07	3/2.65
6	16.26	2/1.99	4/1.98
6	18.06	3/1.33	3/2.65
7	16.18	2/1.97	5/1.59
7	16.62	3/1.32	4/1.98
8	16.34	2/1.95	6/1.32
8	15.94	3/1.30	5/1.59
8	17.64	4/0.98	4/1.98
9	15.62	3/1.29	6/1.32
9	16.50	4/0.97	5/1.59

TABLE II
SPECIFICATION AND PERFORMANCE OF A 30-POLE, 7-PHASE, 100-rpm, 100-kW FRRM

Power rating	100	kW
Force density	40	kN/m^2
Voltage per phase	680	Volts
Air-gap diameter	100.0	cm
Air-gap width	0.1	cm
Axial length	15.20	cm
Number of q-axis phases	5	
Current density,rms	5.86	MA/m^2
Surface current density	118.1	kA/m
Air-gap flux density	0.95	tesla
Copper losses	9.354	kW
Total losses	9.770	kW
Efficiency at rated power	90.23	%
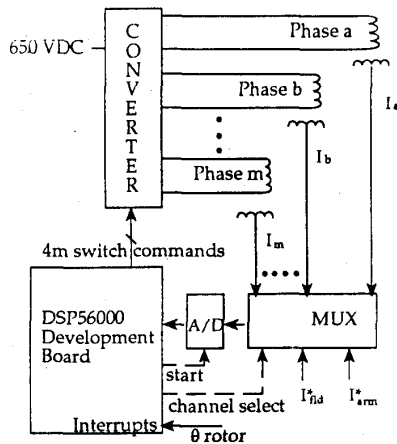
Fig. 6. Block diagram of the converter and controller used to operate the laboratory FRRM.

Fig. 7. Rotor geometry of the experimental FRRM.

Insulated gate bipolar transistors (IGBT's) were used as the power switching devices. Snubbers are not used; however, diode capacitor voltage clamps protect each IGBT. Since the value of a phase current command is dependent on the rotor position and either the d-axis or q-axis current command, six independent software state machines were used to determine the converter switch commands.

The frame, end bells, stator iron, bearings, and shaft of an 1800-rpm, 100-kW squirrel cage induction motor were used as the foundation for the experimental FRRM. The selection of these parameters was made to minimize the need to scale the results in verifying the 40-kN/m², 100-kW design. The bus voltage was selected to be 680 V, the same as that of the 40-kN/m², 100-kW machine.

The selection of the air-gap width was specified at 0.5 mm, one-half that of the 40-kN/m², 100-kW machine, which results in a close magnetic modeling of the 40-kN/m² design. The given slot size results in a surface current density approximately one-half that of the 40-kN/m² design. Keeping approximately the same ratio of field phases to total number of phases means that approximately only one-half the mmf is available to be dropped across the air-gap. Therefore, an air-gap width one-half thta of the 40-kN/m² design was selected resulting in approximately the same air-gap flux density. The choice of rotor magnetic material, 14-mil M6 grain-oriented iron lamiantions, was the same as specified for the rotor of the 40-kN/m², 100-kW machine.

Six poles were chosen for the experimental FRRM to obtain an aspect ratio (stack length/pole pitch) as close as possible to that of the full scale machine. The base electrical frequency was chosen to be 25 Hz, the same as that of the 40-kN/m², 100-kW machine.

The shape of the rotor poles was fixed by factors relating to construction. The pole face pitch to pole pitch was set equal to the ratio of field phases to total number of phases. To ensure mechanical integrity of the rotor,
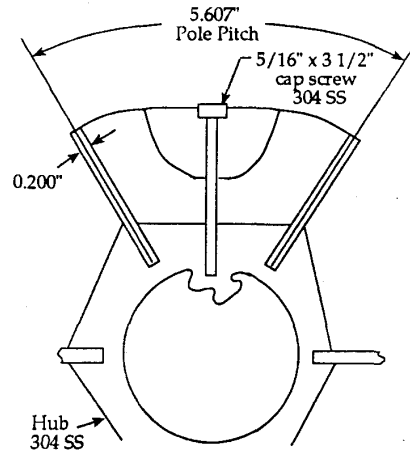
nonmagnetic stainless steel webs were placed in the middle of the pole faces as shown in Fig. 7.

In order to verify the validity of the design procedure, the self- and mutual inductances versus rotor position were measured. Fig. 8 shows both the measured and predicted self- and mutual inductances. A magnetic circuit model program was used to calculate the analytical inductance values. It is apparent that very good correlation was obtained in all cases.

The experimental machine was not tested at rated speed and torque due to a lack of a large enough dynamometer and a limited budget. However, Fig. 9 shows an experimentally obtained current waveform from the laboratory FRRM which is clearly similar to that assumed in the design procedure.

Static torque measurements using dc currents were conducted to verify the force density predictions of the finite-element analysis and the force density equations used in the design. In particular, the correlation of experimentally measured maximum average torque over an electrical angle of 30° versus current with results from finite-element analysis is shown in Fig. 10. The magnitude of the current in field phases and the armature phases was held equal during the determination of the torque data.

VII. CONCLUSIONS

Based on analysis, it has been shown that an FRRM is capable of developing 68% greater force density than an induction machine, based on equal weight of conducting material within the stack, total conduction losses, and peak air-gap flux densities. However, space must be found on the stator for a larger cross-sectional slot area.

An FRRM operating with the same force density, weight of conducting material, and peak air-gap flux density as an induction machine produces 34.4% of the induction motor conduction losses. While not discussed in detail in this paper, it can also be shown [8] that the maximum switch-utilization ratio for a converter supplying an FRRM is 28% higher than the maximum switch-utilization ratio for
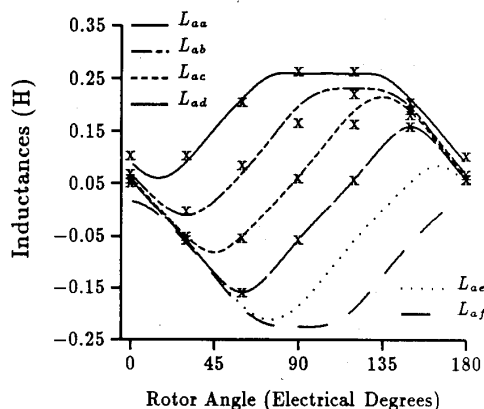
Fig. 8. Comparison of experimentally determined phase inductances with results obtained from a magnetic circuit model.
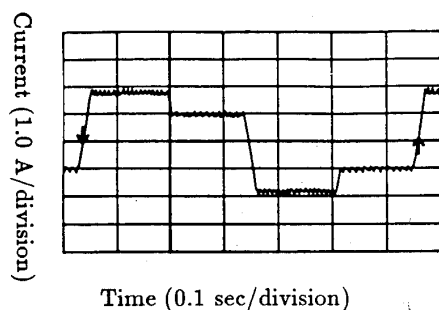

Time (0.1 sec/division)

Fig. 9. Experimentally obtained current waveform from the laboratory FRRM. The d-axis command current is 1.0 A and the q-axis command current is 2.0 A. DC bus voltage = 35 V, fundamental frequency = 1.61 Hz.
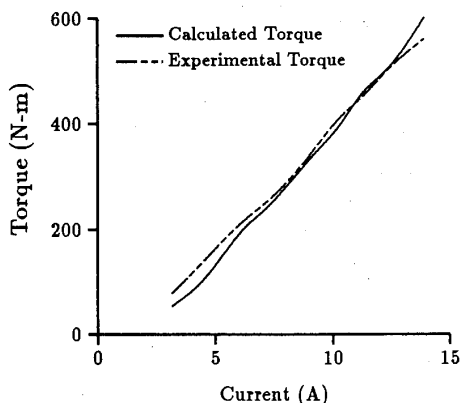

Current (A)

Fig. 10. Maximum average torque over 30° versus current.

an inverter supplying a conventional squirrel cage induction machine.

In addition, the unidirectional rotor flux and absence of rotor conductors in an FRRM result in very low rotor losses. These predictions were backed up by experimental confirmation of the machine models. It is therefore anticipated that such machines could find great utility in motor drives, particularly in large sizes where the additional number of phases does not contribute significant additional cost.

REFERENCES

[1] H. Weh, "On the development of inverter fed reluctance machines for high power densities and high outputs," (in German), Electrical Machines Institute of the Technical University of Brauschweig (FRG), etz Archiv, Bd. 6, pp. 135–14, 1984.
[2] H. Weh and U. Schröder, "Static inverter concepts for multiphase machines with square-wave current-field distributions," in Proc. EPE (Brüssels), Oct. 16–18, 1985, pp. 1147–1152.
[3] J. K. Asper, T. Griender, H. J. Widmer, and J. Mosebach, "Inverter fed 10 kW reluctance machine for flywheel energy storage systems operating at 12,000–24,000 RPM," in 21st IECEC (San Diego, CA), Aug. 1986, pp. 889–894.
[4] R. Mayer, H. Mosebach, U. Schröder, and H. Weh, "Inverter-fed multiphase reluctance machine with reduced armature reaction and improved power density," in Proc. ICE 1986, Munich.
[5] I. Boldea and S. A. Nasar, "Emerging electric machines with axially laminated anisotropic rotors," Electr. Mach. Power Syst., vol. 19, no. 6, pp. 623–703, Nov.–Dec. 1991.
[6] A. J. O. Cruickshank, R. W. Menzies, and A. F. Anderson, "Axially laminated anisotropic rotors for reluctance machines," Proc. IEE, vol. 113, no. 12, pp. 2058–2060, 1966.
[7] R. Schiferl, "Design considerations for salient pole, permanent magnetic synchronous motors in variable speed drive applications," Ph.D. thesis, Univ. Wisconsin-Madison, 1987.
[8] J. D. Law, "Modeling of field regulated reluctance machines," Ph.D. thesis, Univ. Wisconsin-Madison, 1991.
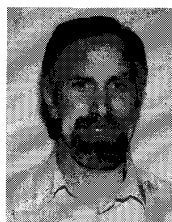
Joseph D. Law (S'85–M'91) was born in Madison, WI on October 27, 1957. He received the B.S.E.E. degree in 1981 from the University of Idaho and the M.S. and Ph.D. degrees in electrical engineering from the University of Wisconsin-Madison in 1985 and 1991, respectively.

He was an Electrical Engineer in the Research Division of Carrier Corporation, Syracuse, NY in 1984 and 1985. He joined the University of Idaho as an Assistant Professor in 1989. He is currently the Lead of the Advanced Transportation Systems Group of the National Center for Advanced Transportation at the University of Idaho. His current work is with ac traction for rail, packaging and thermal management of power semiconductors, high-speed machine design, and magnetic circuit modeling of machines.

Allan Chertok (S'57–M'62) received the B.S.E.E. and M.S.E.E. degrees from New York University in 1961 and 1962, respectively.

While at EG & G from 1962–1970, he was engaged in the development of optical scanners, xerographic printing mechanisms, and automatically equalized modems for advanced digital facsimile terminals as well as in the development of data storage/retrieval and instrumentation systems. Mr. Chertok was a founder of Concord Computing Corporation and from 1970–1979 directed the development of regional and nation-wide data communication networks, voice response servers, and transaction terminals for a retail credit authorization service. Mr. Chertok joined U.S. Windpower (USW) during its start-up phase in 1979 and directed the development of generator, control, and SCADA systems as well as turbine blade pitch actuators and power control algorithms for 100-kW fixed speed turbines. At USW he also played a key role in formulating the generator and power electronic systems architecture for an advanced 300-kW variable speed turbine and directed the development of a battery energy storage system which enabled integration of wind turbines with an isolated diesel power plant. Mr. Chertok was a co-founder of the CERTEK Corporation in 1991 and has since been engaged in the development of large, high-performance, permanent magnet machines and power electronic interfaces for various industrial and government applications.

He is a Registered Professional Engineer and a member of the IEEE Industry Applications Society. Mr. Chertok holds 10 U.S. and related foreign patents related to data and facsimile transmission, data storage/retrieval, and wind turbine control.

Thomas A. Lipo (M'64–SM'71–F'87) is a native of Milwaukee, WI. He received the B.E.E. and M.S.E.E. degrees from Marquette University, Milwaukee, WI in 1962 and 1964 and the Ph.D. degree in electrical engineering from the University of Wisconsin in 1968.

From 1969 to 1979 he was an Electrical Engineer in the Power Electronics Laboratory of Corporate Research and Development of the General Electric Company, Schenectady, NY. He became Professor of Electrical Engineering at Purdue University in 1979 and in 1981 he joined the University of Wisconsin in the same capacity where he is presently the W. W. Grainger Professor for Power Electronics and Electrical Machines.

Dr. Lipo has been engaged in power electronics research for over 25 years. He has received 11 patents and has 16 IEEE prize paper awards for his work, including co-recipient of the Best Paper Award in the IEEE Industry Applications Society Transactions for the year 1984. In 1986 he received the Outstanding Achievement Award from the IEEE Industry Applications Society for his contributions to the field of ac drives and in 1990 he received the William E. Newell Award of the IEEE Power Electronics Society for contributions to the field of power electronics. He is currently the President of the IEEE Industry Applications Society.